

pubs.acs.org/JACS Article

Thiol—Ene Networks from Sequence-Defined Polyurethane Macromers

Emily A. Hoff, Guilhem X. De Hoe, Christopher M. Mulvaney, Marc A. Hillmyer, and Christopher A. Alabi*



Cite This: https://dx.doi.org/10.1021/jacs.0c00759



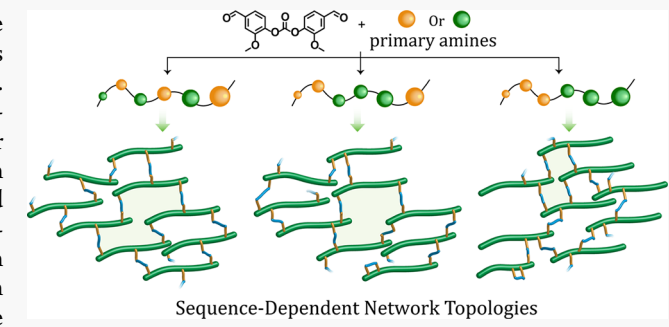
ACCESS

III Metrics & More

Article Recommendations

Supporting Information

ABSTRACT: To date, scalability limitations have hindered the exploration and application of sequence-defined polymers in areas such as synthetic plastics, fibers, rubbers, coatings, and composites. Additionally, the impact of sequence on the properties of cross-linked networks remains largely unknown. To address the need for synthetic methods to generate sequence-defined materials in gram quantities, we developed a strategy involving inexpensive and readily functional vanillin-based monomers to assemble sequence-defined polyurethane oligomers via sequential reductive amination and carbamation. Three oligomers were synthesized with monomer sequence precisely dictated by the placement of reactive side chains during the reductive amination reaction. Avoiding



excessive chromatographic purification and solid- or liquid-phase supports enabled synthesis of sequence-defined oligomers on the gram-scale. Remarkably, sequence was shown to influence network topology upon cross-linking, as evidenced by sequence-dependent rubbery moduli values. This work provides one of the first examples of a scalable synthetic route toward sequence-defined thermosets that exhibit sequence-dependent properties.

■ INTRODUCTION

Innovations in new polymeric material development have led to exciting and breakthrough technologies in fibers and fabrics, high-value coatings, dental materials, personal and military protection, and much more. 1,2 Polymeric materials such as polyurethanes used in applications that require high strength, solvent resistance, and high-temperature performance traditionally employ thermosets. 1,3,4 Thermosets are classically made by cross-linking either long polymer chains or multifunctional small molecules. High cross-link densities and extensive percolated networks are often responsible for high moduli at service temperature and superior performance even under harsh chemical environments. 1,5,6 In addition to crosslink density, the distribution of cross-links, i.e. network topology, is a strong determinant of material property. Because most cross-linking reactions are kinetically controlled (e.g., condensation and radical-based reactions), formation of kinetically trapped states is dictated in part by sterics and thus highly dependent on the geometry of the multifunctional molecule or distribution of cross-linking groups in the polymer chain. It follows that the relative position or sequence of crosslinkable groups in a polymeric chain, particularly in a rigid chain, should affect the kinetics of cross-linking, the conformation of kinetically trapped states, and thus the network structure and material properties. However, due to the synthetic challenges associated with creating precision

polymers at scale, little is known regarding how molecular geometry or functional group spacing, especially in rigid backbones, affect network connectivity.

Following our previous studies with sequence-defined oligothioetheramides (oligoTEAs) on the effect of backbone and pendant group sequence on biological properties, 7-10 we reasoned that sequence should also influence the properties of networks used in materials science. We were particularly inspired by recent reports from Johnson and coworkers on unimolecular stereoisomeric block copolymers (BCP) created via the iterative exponential growth (IEG) method at gram scale.11 X-ray scattering experiments showed that the stereochemical sequence alone could be used to tune bulk morphology. Although IEG is limited to repetitive or palindromic sequences, it allows for gram-scale preparation and is the first platform to show the influence of stereochemical sequence in unimolecular polymers on bulk material morphology. Another example is the pioneering work by Meyer and coworkers who exploited the influence of sequence

Received: January 20, 2020 Published: March 23, 2020



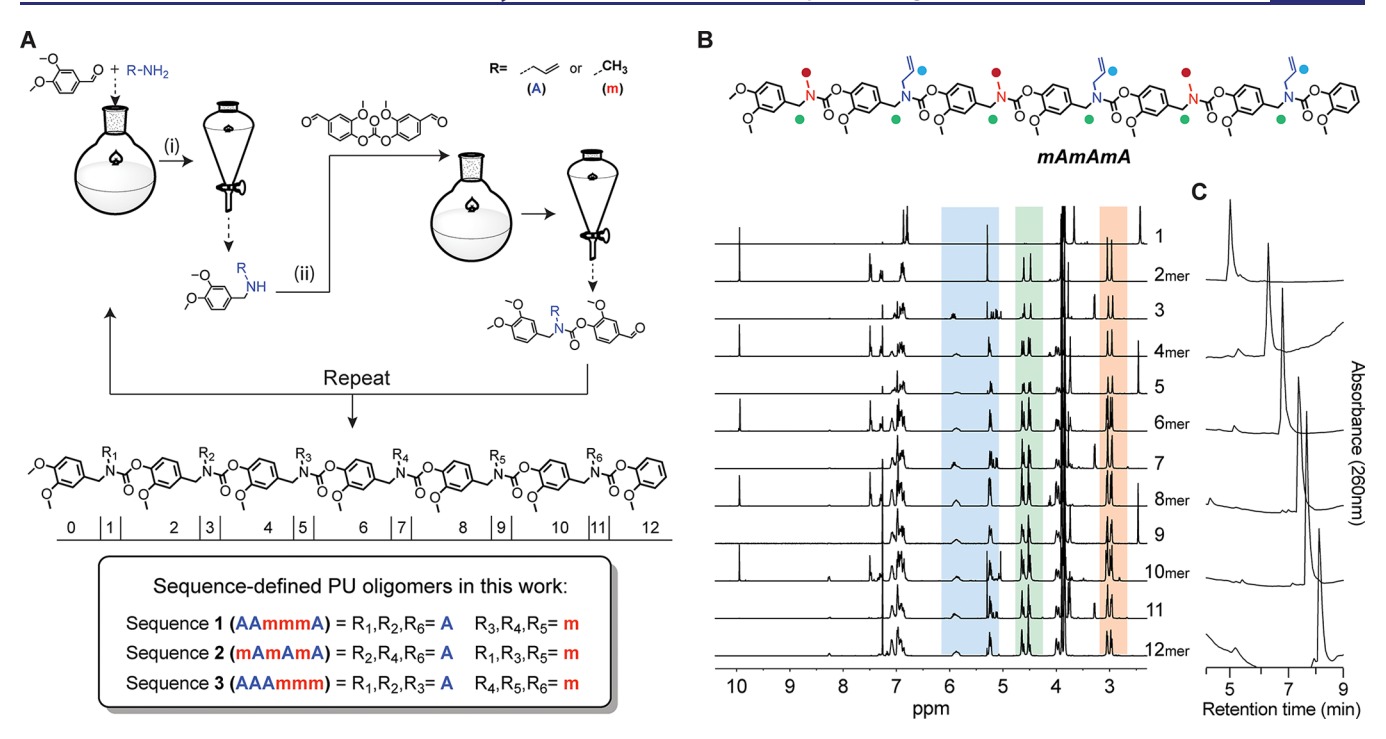


Figure 1. (A) General synthesis scheme for scalable manufacturing of sequence-defined polyurethane macromers: (i) methanol, Na₂SO₄, 2.5 h at RT, then NaBH₄, 0 °C to RT in 1 h; (ii) triethylamine, CH₃CN, 50 °C. (B) ¹H NMR progression of SD-PUM synthesis and (C) SD-PUM synthesis progression monitored via liquid chromatography.

on the hydrolysis profile of a synthetic, albeit polydisperse polymer, poly(lactic-co-glycolic acid) (PLGA). ¹² In both examples, a process that produced gram-scale amounts of material had to be developed to examine the influence of sequence on self-assembled copolymers and thermoplastics. Addressing the question of how sequence affects the network connectivity in thermosets, however, has not been done and requires studying network formation with well-defined and easily accessible functional macromolecules.

Creating synthetic polymeric chains with a dispersity of one remains a major challenge in the field of polymer chemistry. A variety of iterative addition techniques, which involve addition of one monomer at a time to the end of a growing polymer chain followed by purification, have been employed to give short sequence-defined polymer compositions with a dispersity of 1.13-23 Iterative addition on the solid phase via insoluble beads facilitates rapid purification but can be difficult to scale up due to surface area limitations. Alternatively, several research groups, including our lab, have proposed liquidphase iterative synthetic methods to bypass these limitations. These methods encompass the use of "liquid polymeric/ organic supports" or support-free techniques that accomplish purification between each step via chromatography techniques. Despite the advantages of rapid solution phase kinetics, scale up of "liquid support" systems is limited by significant purification losses and high cost of fluorous tags or prepolymer supports. Methods that do not involve any supports are highly promising due to their direct pathway for scale up. Few have explored this path, and notable recent examples include efforts by Meier, ^{24,25} Johnson, ^{26,27} and Livingston. ²

Herein, we describe a versatile strategy to synthesize sequence-defined polyurethane macromers (SD-PUM) derived from the biorenewable monomer, vanillin, via a support-free strategy on the gram-scale. Key advantages of this strategy include iterative assembly without a support, inexpensive

monomers, high-yielding reactions, and simple liquid—liquid extraction for stepwise purification. Three unique fluorescent SD-PUM isomers were created at the 2–5 g scale bearing reactive allyl and nonreactive methyl pendant groups. Notably, the gram-scale synthesis of SD-PUMs with precise sequence definition enabled the study of structure—property relationships with respect to how sequence affects the thermal and mechanical properties of the final cross-linked networks. Our studies revealed that a block SD-PUM sequence shows less favorable thermal and mechanical properties relative to its other sequence isomers, thus confirming the importance of sequence on the properties of cross-linked materials. Access to this type of investigation will contribute to fundamental design principles for future applications in high-performance materials.

■ RESULTS AND DISCUSSION

Synthesis of SD-PUMs. We chose vanillin as the basis of SD-PUM backbones because it is biorenewable, inexpensive, possesses advantageous functional groups for orthogonal synthesis, and will contribute to a relatively rigid polymeric backbone. The benzylic aldehyde of vanillin reacts readily with widely available primary amines to generate a useful secondary amine handle. Furthermore, the phenol of vanillin is easily converted to a reactive carbonate, divanillin carbonate, on a large scale (~ 60 g). Carbamate backbone units were formed by reacting divanillin carbonate with the secondary amine termini generated via reductive amination.

Preparation of each SD-PUM began by reacting 3,4-dimethoxybenzaldehyde with the first desired primary amine via a reductive amination reaction to generate a secondary amine. After purification via a simple aqueous wash, divanillin carbonate was then reacted with the secondary amine to give a substituted carbamate with a new aldehyde site which can be used for the next reductive amination step (Figure 1A). This

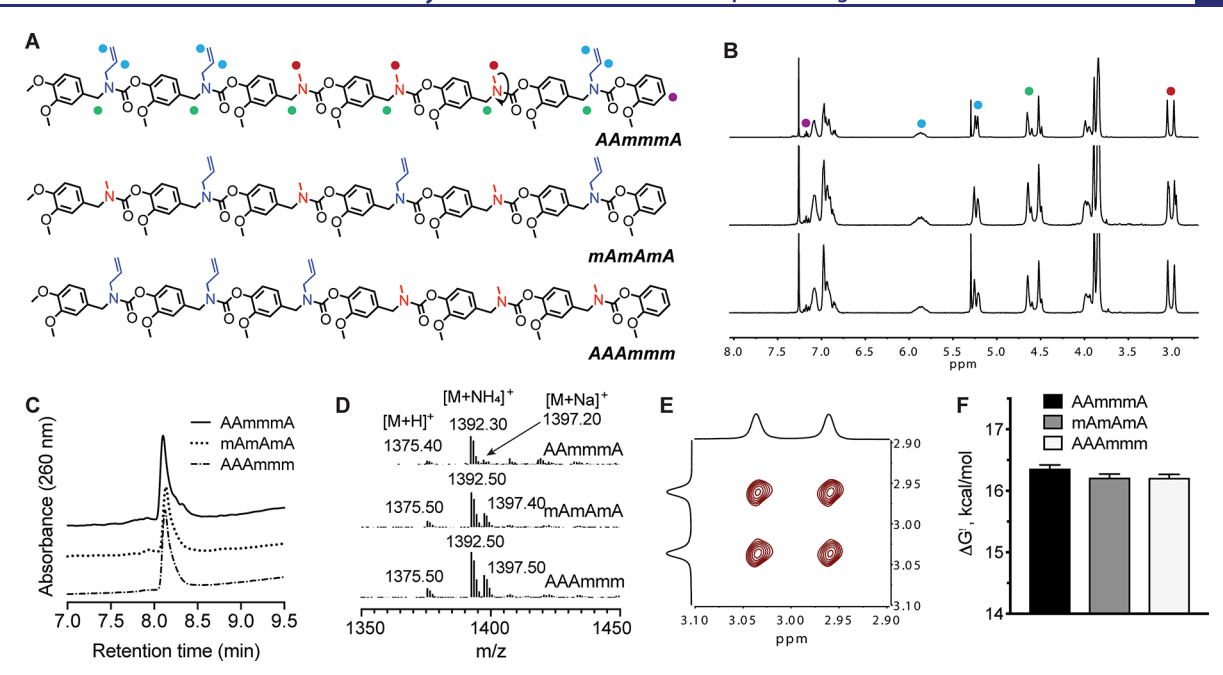


Figure 2. (A) SD-PUM structures. (B) ¹H NMR of the isomeric 12-mers. (C) Retention time of SD-PUMs on a C4 reverse-phase column (Supplementary Figure 1 shows the spectra with an expanded baseline). (D) Mass spectra of isomeric SD-PUMs. (E) 2D EXSY spectra at 200 ms mixing time for AAmmmA. (F) The off-diagonal peaks in the 200 ms EXSY spectra were used to calculate the rate constants for conformer exchange. The Gibbs free energy of activation was calculated directly from the rate constant and the Eyring equation.

carbamate formation generates vanillin as a byproduct, which is water-soluble, and the excess divanillin carbonate can be hydrolyzed to vanillin using an ammonium hydroxide solution. An alkaline-aqueous workup is then sufficient to remove the vanillin and ammonium hydroxide byproducts. The symmetric carbonate of vanillin was used for each carbamation step (excluding the final capping carbamation) because it yielded exclusively vanillin-derived carbamates. An additional benefit of using this monomer is the potential for recycling vanillin. Optimization of these synthesis and purification steps enables the production of precision SD-PUMs at scale with only a round-bottom flask, a separatory funnel for purification, and a rotovap for solvent removal for the majority of steps (Figure 1A). In the last step of the oligomer formation, divanillin carbonate was substituted with a 4-nitrophenyl-activated carbonate of guaiacol, an analogue to vanillin without the aldehyde, to provide a nonreactive end-group. The final amination and carbamation steps were purified by column chromatography.

The side chain sequence was varied by changing the order of primary amines used in the reductive amination steps, while the vanillin-based backbone was kept constant. So far, methyl (nonreactive) and allyl (reactive) substituents have been used as pendant groups to give three distinct, monodisperse, and constitutionally isomeric sequence-defined macromers in 2-5 g quantities (Figure 1A). Each oligomer is named for its sequence of side chains, where m represents a methyl substituent and A represents an allyl substituent. The allyl functional groups were selected to enable cross-linking of each oligomer via thiol-ene chemistry. Three sequences were selected for investigation: an alternating sequence (mAmAmA), a block sequence (AAAmmm), and a comparative "disordered" sequence (AAmmmA) (Figure 1A). The modularity of the monomers and reactions used in the preparation of SD-PUMs ensure that this platform can be used

to produce highly multifunctional scaffolds in addition to the binary macromers in this report.

The progression of each SD-PUM synthesis was followed by ¹H NMR spectroscopy and liquid chromatography mass spectrometry (LC-MS). As an example, the ¹H NMR spectra at each step during preparation of mAmAmA are shown in Figure 1B. As shown in Figure 1A, the 1-mer represents the product of the first reductive amination step, i.e. 3,4dimethoxy-N-methylbenzylamine. After each carbamation reaction with divanillin carbonate, the aldehyde peak at 10 ppm appears and after each reductive amination step, the aldehyde peak disappears. Similarly, the resonance of the Nmethyl group in the N-methylbenzylamine adducts shifts from 2.45 to 3 ppm (Figure 1B, 1 vs 2mer, 5 vs 6mer, and 9 vs 10mer), and the methylene proton signals shift from 3.7 to 4.6 ppm upon carbamation (Figure 1B). The synthesis process was also monitored by LC-MS equipped with a diode-array detector for simultaneous absorbance and mass analysis. A consistent shift toward longer retention times with each monomer addition (Figure 1C) was observed. The absorbance and molecular ion peak for each addition step corresponded to the desired mass as shown in Supplementary Table 1. The final yield of the three 12-mer isomers (Figure 2A) ranged from 7-10%. Even at these overall yields, sequence-defined macromers were produced on a multigram scale with inexpensive regents and minimal chromatographic purification. As such, we present this synthetic strategy as a scalable route to sequence-defined oligomers that enables evaluation of sequence effects in applications (e.g., cross-linked networks) where gram quantities are required.

The ¹H and ¹³C NMR spectra of all three SD-PUM sequences shared similar spectral features with minor differences in splitting patterns around the *N*-methyl protons (Figure 2B and Supplementary Figures 2–4). The three isomers also displayed a similar retention time (i.e., relative hydrophobicity) when run on a reverse phase C4 column

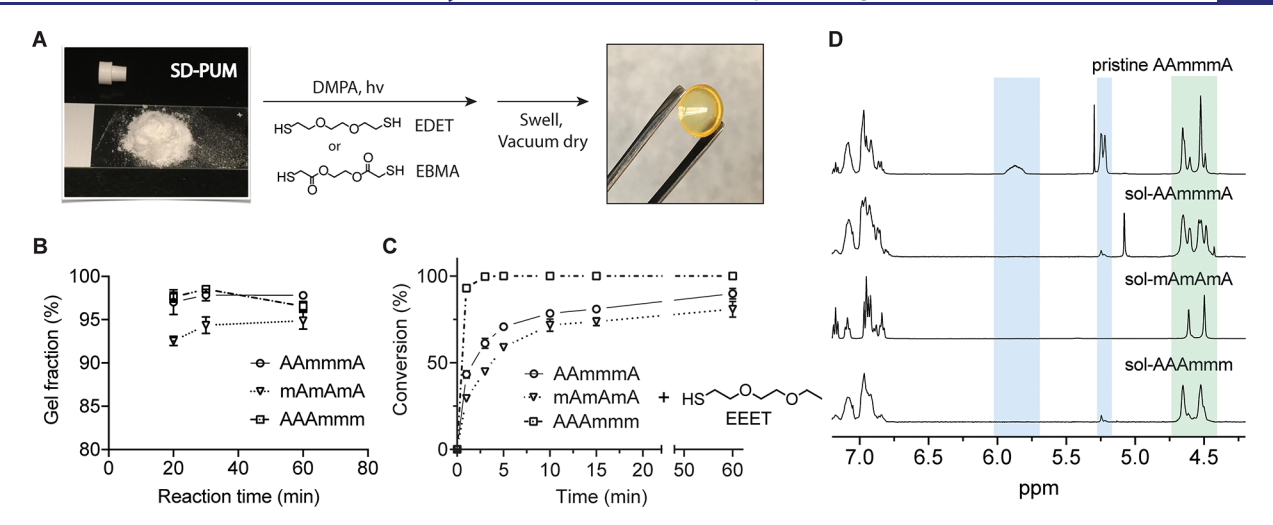


Figure 3. (A) Representative images of a SD-PUM that is then solvent cast and cross-linked via photoinitiated thiol—ene reaction with EDET or EBMA and the resulting free-standing film. (B) Gel fraction obtained for each cross-linked oligomer at different UV-curing times. The 20 and 30 min time point measurements were done in experimental duplicates, while the 60 min time points were done in triplicate. The error bars represent the standard deviation from the experimental replicates (three technical replicates per measurement). (C) Solution phase thiol—ene reaction kinetics of SD-PUMs with EEET monitored by the disappearance of allyl peaks at 5.23 and 5.86 ppm by ¹H NMR spectroscopy. The lines drawn between the symbols are only meant to show the trends in the data. (D) ¹H NMR characterization of sol-extract from SD-PUM/EDET networks compared to pristine AAmmmA SD-PUM. The blue region highlights the olefin peaks, while the green region highlights the protons alpha to the urethane bond.

(Figure 2C), and all gave identical mass spectra (Figure 1D) with the desired molar mass ($[M + H]^+ = 1375.5 \ m/z$, $[M + NH_4]^+ = 1392.5 \ m/z$, and $[M + Na]^+ = 1397.5 \ m/z$).

Conformational Exchange of SD-PUMs. While monitoring the progress of oligomer synthesis via 1H NMR spectroscopy, strong splitting patterns evolved for backbone methylene and carbamate methyl peaks (Figures 1B and 2B) that suggested different conformational populations of methylene and carbamate methyl groups due to slow rotation around the C(O)-N bond. The two peaks for the methyl group at ~ 3 ppm arise due to the differential positioning of the protons on the methyl group relative to the aromatic group, resulting in a more deshielded proton signal when the position is closer to the aromatic group.

To probe the solution conformational dynamics of each macromer, a two-dimensional homonuclear exchange spectroscopy (¹H-¹H EXSY) experiment was conducted for each oligomer at 0 and 200 ms mixing times. A representative 2D NMR spectrum at 200 ms for AAmmmA is shown in Figure 2E. Complete 2D spectra for the other macromers at 0 and 200 ms can be found in Supplementary Figures 5-7. The appearance of off-diagonal EXSY peaks in the 200 ms spectra for each SD-PUM confirmed the presence of slow conformational exchanges between the different positions. The rate constants for conformational exchange were calculated with the program EXSYcalc by integrating the diagonal and EXSY peaks in each spectrum. The Gibbs free energy of activation (ΔG^{\dagger}) for each SD-PUM was then determined via the Eyring eq (Supplementary Eq 1) using the forward rate constant and was found to be \sim 16.3 kcal/mol across sequences (Figure 1F). This ΔG^{\ddagger} is on par with values obtained for hindered internal rotation in N,N-dialkyl amides. 29,30 Variable temperature NMR (VT-NMR) was also used to infer the conformational dynamics of each SD-PUM. As the temperature was increased from 25 to 100 °C, the coalescence of the two methyl and methylene peaks at 4.6 and 3 ppm, respectively, into one broader set of peaks for each was indicative of hindered C-N

rotation. The transition occurred at 60 $^{\circ}$ C for all three sequences (Supplementary Figure 8–10). These results imply that the macromers exhibit hindered rotation around the C(O)-N carbamate bond.

Effect of Sequence on Network Formation. Prior to cross-linking, the thermal stability of each pure SD-PUM was determined by thermogravimetric analysis (TGA) (Supplementary Figure 11). The thermal stability of each oligomer, as assessed by mass loss, did not vary significantly across sequences. Less than 5% mass loss was observed below 280 °C, which is attributed in part to moisture and solvent evaporation. To probe how sequence may affect material properties, we exploited the allyl groups in the SD-PUMs to create cross-linked networks. Networks were prepared by solvent casting a mixture of each SD-PUM, a dithiol crosslinker [(2,2'-(ethylenedioxy)diethanethiol (EDET) or ethane-1,2-diyl bis(2-mercaptoacetate) (EBMA)], and a photoinitiator (2,2-dimethoxy-2-phenylacetophenone (DMPA)) in acetonitrile into the circular wells (100 mm in diameter × 1 mm deep) of a PTFE mold. The dithiol cross-linkers were selected for their commercial availability, miscibility with the SD-PUMs in solution, and similar chain lengths to aid in network comparisons. A representative image of a SD-PUM powder (prior to solvent casting) cross-linked to give a freestanding disc is shown in Figure 3A. Cross-linking was initiated with UV light (365 nm, 20 mW/cm²), and several curing times (20, 30, and 60 min) were investigated to provide kinetic profiles of curing for each sequence. After the cross-linking reactions, each film was removed from the mold and immersed in acetonitrile for 48 h to remove unincorporated monomers and photoinitiator from each network. Once the soluble (sol) fractions were removed, the films were dried in a vacuum oven for 16 h at 100 °C.

The strong UV absorption of the SD-PUMs (Figure 2C) led us to investigate their fluorescence emission upon excitation with UV light. All three macromers exhibited intrinsic fluorescence at 306 nm following excitation at 270 nm. After

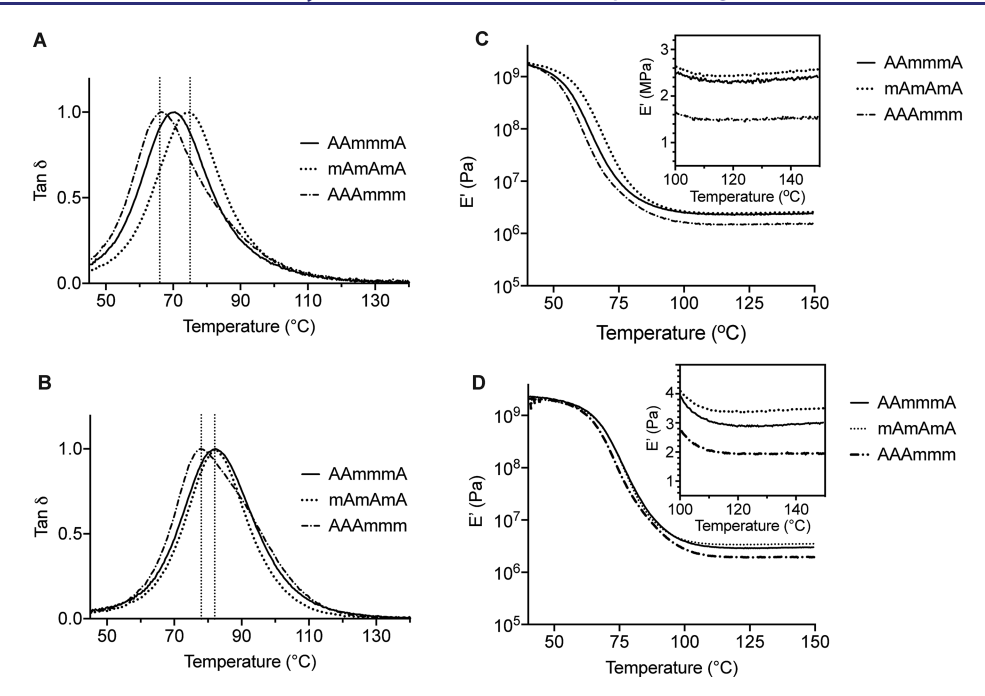


Figure 4. Thermal and mechanical properties of sequence-controlled networks (60 min UV-cure). (A–D) DMTA of each cross-linked network. The tan δ curves are shown for (A) the EDET cross-linked networks and (B) EBMA cross-linked networks; dotted lines correspond to the peak maxima for the AAAmmm and mAmAmA networks. (C) Plots of storage modulus (log scale) as a function of temperature for EDET cross-linked networks; the inset shows a zoomed in view of the rubbery regime. (D) Plots of storage modulus (log scale) as a function of temperature for EBMA cross-linked networks; the inset shows a zoomed in view of the rubbery regime.

generating calibration curves for each sequence, fluorescence measurements were used to determine the amount of unincorporated SD-PUM, independent from the amount of thiol-based cross-linker (reacted or unreacted) or initiator, in the sol fraction at each curing time point; the corresponding gel fractions were then calculated by subtracting the sol fractions from the total amount of SD-PUM (Figure 3B). We confirmed in separate experiments that the consumption of allyl groups via the thiol-ene reaction did not significantly affect the fluorescence quantum yield. Moreover, gel fraction data obtained by gravimetric analysis were similar (albeit slightly higher due to the contribution of the cross-linker mass) to those obtained by fluorescence measurements (Supplementary Figure 15). The gel fraction data in Figure 3B indicate that the AAmmmA and AAAmmm sequences have slightly faster reaction kinetics relative to the mAmAmA sequence. Reaction times below 20 min did not yield intact films and precluded the acquisition of early stage gel fraction kinetics via the use of sol fraction fluorescence measurements. To further explore the early stage reaction kinetics, we performed control experiments where the SD-PUMs were reacted with a monothiol, 2-(2-ethoxyethoxy)ethane-1-thiol (EEET) under the same conditions as the cross-linking reaction. The disappearance of the allyl group was monitored by ¹H NMR spectroscopy (Supplementary Figure 12-14), and the conversion was plotted as a function of time (Figure 3C). In this experiment, we observed that the AAAmmm sequence had the fastest thiol-ene reaction kinetics, followed by the AAmmmA, and the mAmAmA sequence was again the slowest. We postulate that oligomer conformation or a local concentration effect is responsible for the faster reaction kinetics of the AAAmmm sequence. To the best of our knowledge, thiol-ene modification of sequence-defined systems such as ours have not been demonstrated, and

computational studies are underway to provide additional information to test the aforementioned assertions. Due to peak overlap in the ¹H NMR spectra, it was not possible to reliably quantify thiol conversion, but qualitatively, the thiol peak at 1.6 ppm seemed to disappear at similar rate as the alkene peaks at 5.2 and 6 ppm.

Although the SD-PUMs had minor differences in reaction kinetics with EEET, all sequences reached a similar gel fraction of 95-97% after 60 min of irradiation (Figure 3B). With this near complete SD-PUM incorporation into the network and relatively fast reaction kinetics (Figure 3C), we posited that all of the alkenes in the network were fully reacted. To indirectly address this supposition, we probed the sol fraction of the AAmmmA, mAmAmA, and AAAmmm films after 60 min of curing with ¹H NMR spectroscopy (Figure 3D). The ¹H NMR of the sol-fraction showed that in all cases, virtually all allyl groups were reacted as evidenced by the dearth of olefin peaks between 5.2 and 6 ppm (Figure 3D, highlighted blue region, less than 0.1% remaining at 5.2 ppm). We suspect the reacted oligomers in the sol fraction are likely cyclic products or the result of having a small excess of cross-linker in the reaction. Identification of these individual structures using NMR spectroscopy and LC-MS proved inconclusive. This result, along with the gel fraction data in Figure 3B, indirectly suggests that all three networks have similar extents of crosslinking at the 60 min irradiation time point. Following the gelfraction data in Figure 3B that indicated near complete network conversion after 60 min, additional networks using the EBMA cross-linker were also cured for 60 min. Gel fraction analyses (by fluorescence and gravimetric analysis) of these networks also showed near complete SD-PUM incorporation (Supplementary Figure 16).

Effect of Sequence on Thermal and Mechanical Properties of Cross-Linked Networks. The thermal

properties of each EDET or EBMA cross-linked film were evaluated by differential scanning calorimetry (DSC) (Supplementary Figures 17A and 17B). All sequences show similar broad endotherms (Supplementary Figure 17A). The broadness of the endotherm and thus T_g measured by DSC is likely due to the variety of segmental motions in the amorphous sample that results in broad endotherms. For broad endotherms, small changes in heat capacity can be difficult to detect and can obscure subtle differences between samples. The tan delta (tan δ), or the ratio of E' to E'', depicts maxima during thermal transitions and is therefore a common and often more sensitive way to define the $T_{\rm g}$ of a material. To assess the T_{g} and mechanical properties of our networks, larger films were prepared and cut into rectangular tensile bars for dynamic mechanical thermal analysis (DMTA) experiments (Supplementary Figure 18). The tan δ plots from the DMTA experiments for each network from are shown in Figure 4A for the EDET networks and Figure 4B for the EBMA networks. The T_{σ} obtained from the tan δ maximum of the AAAmmm-EDET network ($T_{\rm g} \sim 66~^{\circ}{\rm C}$) was 9 and 4 $^{\circ}{\rm C}$ lower than that of the mAmAmA- and AAmmmA-EDET networks, respectively (Figure 4A). A similar trend was observed for the EBMA networks: the AAAmmm-EBMA network had a $T_{\rm g}$ of 78 °C, which was 4 °C lower than both mAmAmA- and AAmmmA-EBMA networks (Figure 4B).

The storage modulus was measured as a function of temperature for all six cross-linked films (Figure 4C and 4D). Below T_g , the three films made with the EDET crosslinker had identical glassy moduli of 1.7 GPa. Similarly, the three films made with the EBMA cross-linker had identical glassy moduli of 2.3 GPa, approximately 26% stiffer than the EDET networks. However, in the rubbery regime above $T_{\rm g}$, the network properties differed across each set of films. The rubbery modulus for the AAAmmm-EDET network was ~40 and ~30% lower than that of the mAmAmA- and AAmmmA-EDET networks, respectively (Figure 4C, inset). We surmise that these differences in mechanical properties likely arise from factors influencing network topology, such as loop formation and dangling chain ends that are further discussed in the next section. A similar trend was revealed for the EBMA networks (Figure 4D, inset). Our DMTA findings therefore indicated that both the thermal and mechanical properties of the networks made with the block sequence were distinct from those of the networks made from either the alternating or "disordered" sequence. Additionally, a slight increase in the rubbery modulus and $T_{\rm g}$ across all sequences was observed for EBMA networks due to the less flexible cross-linker when compared to the EDET networks.

In addition to the temperature sweep DMTA data, frequency and strain sweeps were also conducted for each network at a fixed temperature of 150 °C (Supplementary Figures 19–22). The modulus values obtained from these tests were in agreement with those obtained from the DMTA temperature sweeps (Figure 5 and Supplementary Figure 23). Regardless of the dithiol cross-linker used, a statistically significant difference in modulus was observed between the AAAmmm-based networks and the networks made from the other two sequences (Figure 5 and Supplementary Figure 23). To probe the role of sequence dispersity, we prepared a "mixed sequence" containing an equimolar ratio (1:1:1) of each SD-PUM and cured it for 60 min with the EDET cross-linker. The rheological analyses revealed that the modulus of the network made with the "mixed sequence" was similar to the average

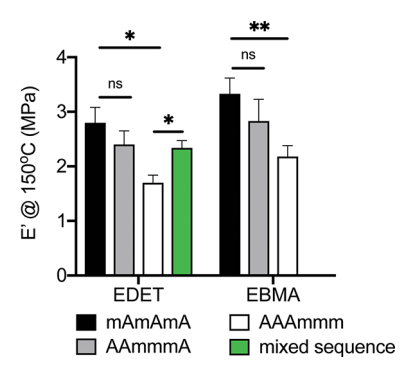


Figure 5. Average storage modulus of each SD-PUM-EDET and EBMA network at 150 °C from the DMTA experiments acquired at a fixed frequency (6.28 rad/s, i.e. 1 Hz) with error bars representing the standard deviation from the mean. The "mixed sequence" is an equimolar ratio of the mAmAmA, AAmmmA, and AAAmmm sequences. All measurements were done in triplicate (i.e., measurement on three sample films) except for the mAmAmA-EDET and AAAmmm-EDET networks, which were done in duplicates (for duplicates the bars represent a range). **, p-value <0.005, *, p-value <0.05.

modulus of all three pristine networks (Figure 5, green bar). The modulus of this "mixed sequence"-EDET network is still higher and statistically different from that of the AAAmmm network. Thus, while subtle, consistent property differences (mechanical and thermal) between networks derived from AAAmmm and those derived from mAmAmA, AAmmmA, and the mixed sequence highlight the role of sequence in dictating the mechanical properties of precision thermoset materials.

Influence of Sequence on Network Topology. While the gel-fraction data and sol-fraction NMR experiments suggested nearly complete network conversions were achieved after 60 min (Figure 3), neither directly examines the conversion of the double bonds within the solid network. To obtain direct information about the network conversion, the EBMA networks containing acid labile ester linkages were subjected to an acidic cleavage solution (trifluoroacetic acid:acetonitrile:water, 1:1:1, v/v/v) for 12 h at 40 °C to achieve complete network degradation (Figure 6A). Cleavage should result in SD-PUMs modified with one, two, or three mercaptoacetic acid (MA) moieties (Figure 6A depicts the mAmAmA sequence modified with three MA moieties) depending on the conversion of the thiol—ene reaction.

The degraded networks were analyzed with LC-MS to identify the extent of MA modification. The LC-MS analyses showed that all sequences predominantly contained the completely modified product (Figure 6B, i.e. Three MA modifications, $[M + H]^+ = 1651 \ m/z$) suggesting near complete conversion of the all double bonds within each network. The mAmAmA sequence with the slowest kinetics (Figure 4B) showed a small amount of the doubly modified product (Figure 4D, ** $[M + H]^+ = 1557 \ m/z$). Additionally, the sol fraction of the EBMA networks was degraded and also showed predominantly modified product (Supplementary Figure 24) with mAmAmA having relatively more species of smaller masses than the other two sequences. These results agree with the sol fraction analyses and support the conclusion that the observed differences in thermal and mechanical properties are related to the impact of sequence on network connectivity, i.e. topology, and not the number of cross-links. Recent reports by Johnson and coworkers on loop formation in

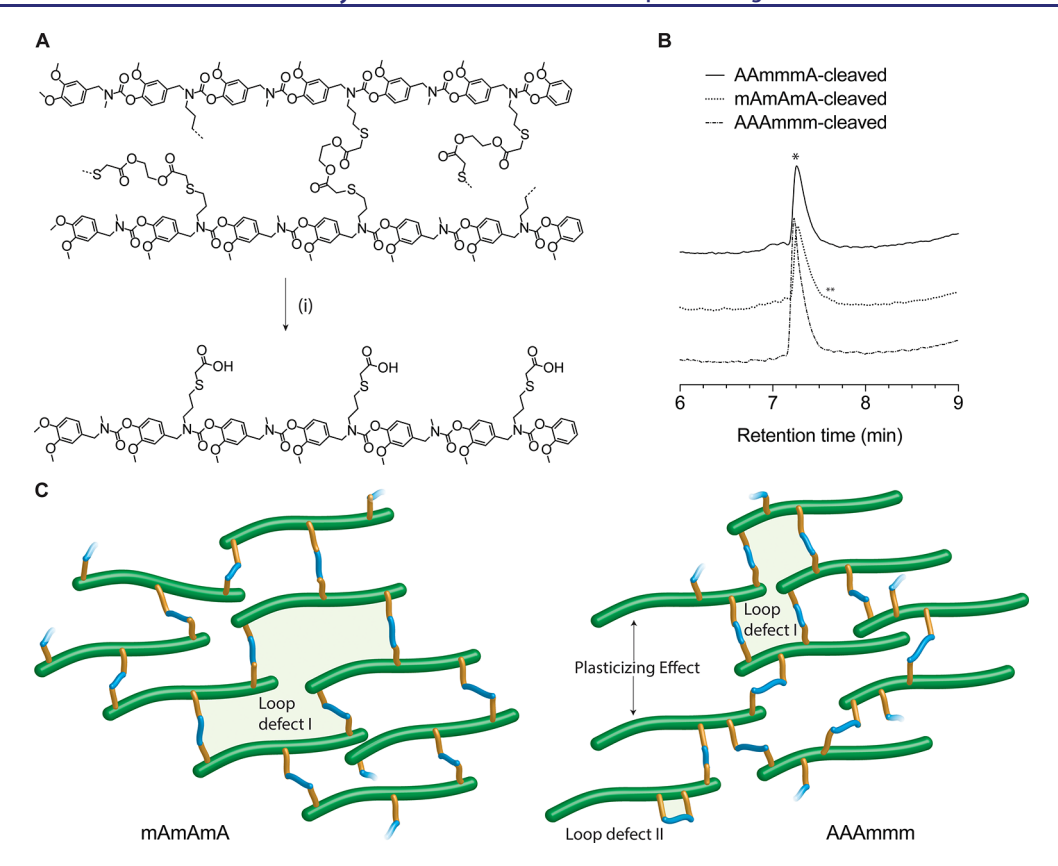


Figure 6. (A) Schematic of model degradable network and a sample degradation fragment after treatment with (i) TFA:CH₃CN:H₂O 1:1:1 v/v/v mixture for 12 h at 40 °C. (B) LC-MS characterization of degradation products after acid treatment. *Corresponds to m/z of 1651 g/mol and **corresponds to m/z of 1557 g/mol. (C) Schematic of mAmAmA and AAAmmm networks labeled with the different types of loops and defects.

cross-linked networks³¹⁻³⁴ suggest that differences in interand intramolecular loop formation may contribute to the differences we see in the AAAmmm networks relative to the other two sequences. Because our gel fraction data and 2D NMR data suggest a similar degree of cross-linking and conformational freedom, respectively, we hypothesize that the observed differences in mechanical behavior may be due to relative amounts of intramolecular loops (Figure, 6C) and dangling chain ends. The presence of elastically ineffective cross-links, such as loops, would explain why we observe similar gel fraction behavior across sequences, but differences in mechanical behavior. It is also possible that the modulus of the AAAmmm networks is lowered by the presence of dangling chain defects (i.e., the mmm segment) throughout the network, as they would also be elastically ineffective network defects³⁵ (Figure 6C). Additionally, differences in overall oligomer conformation could impact resultant network properties. Confirmation of loop structures and conformational differences, however, are beyond the scope of this initial work. Further studies are required to ascertain the relative contributions of loop structures and dangling chains to the network topology and observed mechanical properties.

CONCLUSIONS

With the advent of synthetic sequence-defined polymers, it has become necessary to address both the scalability of sequence-defined materials and their application as tools to better inform our understanding of materials design. In this work, we report one of a few examples of sequence-defined oligomers that can be readily synthesized on a multigram-scale. This was achieved

through the combination of efficient reactions, simple aqueous extractions, and support-free synthesis. Cross-linking of alkene-functional side chains with different dithiols afforded networks with sequence-dependent thermal and mechanical properties. High conversion of the cross-linking reaction was confirmed by gel-fraction and LC-MS analyses, and the sequence-dependent mechanical properties are the result of topological differences related to the SD-PUM microstructure. We propose that loop defects and dangling chain-ends resulting from differences in cross-linkable side chain sequence are primarily responsible for the observed property differences. This study is the first to examine the role sequence definition plays in network topology and will pave the way for explorations of using sequence to tune and control network properties.

ASSOCIATED CONTENT

Supporting Information

The Supporting Information is available free of charge at https://pubs.acs.org/doi/10.1021/jacs.0c00759.

Synthesis and characterization procedures, characterization data of all new compounds, and network data (\mbox{PDF})

AUTHOR INFORMATION

Corresponding Author

Christopher A. Alabi — Robert Frederick Smith School of Chemical & Biomolecular Engineering, Cornell University, Ithaca, New York 14835, United States; oorcid.org/0000-0003-2654-018X; Email: caa238@cornell.edu

Authors

- Emily A. Hoff Robert Frederick Smith School of Chemical & Biomolecular Engineering, Cornell University, Ithaca, New York 14835, United States; orcid.org/0000-0003-3041-9489
- **Guilhem X. De Hoe** − Department of Chemistry, University of Minnesota, Minneapolis, Minnesota 55455-0431, United States; © orcid.org/0000-0002-0996-7491
- Christopher M. Mulvaney Robert Frederick Smith School of Chemical & Biomolecular Engineering, Cornell University, Ithaca, New York 14835, United States
- Marc A. Hillmyer Department of Chemistry, University of Minnesota, Minneapolis, Minnesota 55455-0431, United States; orcid.org/0000-0001-8255-3853

Complete contact information is available at: https://pubs.acs.org/10.1021/jacs.0c00759

Notes

The authors declare no competing financial interest.

ACKNOWLEDGMENTS

Financial support for E.H., C.M., and C.A. was provided by the Army Research Office under award number W911NF-15-10179. Support for G.D.H. and M.H. was provided by the Center for Sustainable Polymers under award number CHE-1413862. G.D.H. also acknowledges the University of Minnesota Doctoral Dissertation Fellowship. This work made use of the Cornell University NMR Facility, which is supported, in part, by the NSF under award number CHE-1531632. The authors thank the Coates group for access to their DSC.

REFERENCES

- (1) Guo, Q. Thermosets 2012, 1.
- (2) Srinivasan, A.; Bandyopadhyay, S. Advances in Polymer Materials and Technology; CRC Press, 2016.
- (3) Pascault, J.-P.; Sautereau, H.; Verdu, J.; Williams, R. J. J. Thermosetting Polymers; CRC Press, 2002.
- (4) Thomas, S.; Datta, J.; Haponiuk, J.; Reghunadhan, A. Polyurethane Polymers: Blends and Interpenetrating Polymer Networks; Elsevier, 2017.
- (5) Auvergne, R.; Caillol, S.; David, G.; Boutevin, B.; Pascault, J.-P. Biobased thermosetting epoxy: present and future. *Chem. Rev.* **2014**, *114*, 1082–1115.
- (6) Handbook of Thermoset Plastics; William Andrew Publishing, 2014, p xxi.
- (7) Porel, M.; Thornlow, D. N.; Artim, C. M.; Alabi, C. A. Sequence-Defined Backbone Modifications Regulate Antibacterial Activity of OligoTEAs. ACS Chem. Biol. 2017, 12, 715–723.
- (8) Hoff, E. A.; Artim, C. M.; Brown, J. S.; Alabi, C. A. Sensitivity of Antibacterial Activity to Backbone Sequence in Constitutionally Isomeric OligoTEAs. *Macromol. Biosci.* **2018**, *18*, e1800241.
- (9) Brown, J. S.; et al. Antibacterial isoamphipathic oligomers highlight the importance of multimeric lipid aggregation for antibacterial potency. *Commun. Biol.* **2018**, *1*, 220.
- (10) Phan, N. N.; Li, C.; Alabi, C. A. Intracellular Delivery via Noncharged Sequence-Defined Cell-Penetrating Oligomers. *Bioconjugate Chem.* **2018**, 29, 2628–2635.
- (11) Golder, M. R.; et al. Stereochemical Sequence Dictates Unimolecular Diblock Copolymer Assembly. *J. Am. Chem. Soc.* **2018**, *140*, 1596–1599.
- (12) Li, J.; Stayshich, R. M.; Meyer, T. Y. Exploiting sequence to control the hydrolysis behavior of biodegradable PLGA copolymers. *J. Am. Chem. Soc.* **2011**, *133*, 6910–6913.

- (13) Porel, M.; Alabi, C. A. Sequence-Defined Polymers via Orthogonal Allyl Acrylamide Building Blocks. *J. Am. Chem. Soc.* **2014**, *136*, 13162–13165.
- (14) Boeijen, A.; Liskamp, R. M. J. Solid-Phase Synthesis of Oligourea Peptidomimetics. *Eur. J. Org. Chem.* **1999**, 1999, 2127–2135.
- (15) Edwardson, T. G. W.; Carneiro, K. M. M.; Serpell, C. J.; Sleiman, H. F. An efficient and modular route to sequence-defined polymers appended to DNA. *Angew. Chem., Int. Ed.* **2014**, 53, 4567–4571.
- (16) Lutz, J.-F.; Ouchi, M.; Liu, D. R.; Sawamoto, M. Sequence-controlled polymers. *Science* 2013, 341, 1238149.
- (17) Martens, S.; Van den Begin, J.; Madder, A.; Du Prez, F. E.; Espeel, P. Automated Synthesis of Monodisperse Oligomers, Featuring Sequence Control and Tailored Functionalization. *J. Am. Chem. Soc.* **2016**, *138*, 14182–14185.
- (18) Grate, J. W.; Mo, K.-F.; Daily, M. D. Triazine-Based Sequence-Defined Polymers with Side-Chain Diversity and Backbone-Backbone Interaction Motifs. *Angew. Chem., Int. Ed.* **2016**, *55*, 3925–3930.
- (19) Espeel, P.; et al. Multifunctionalized Sequence-Defined Oligomers from a Single Building Block. *Angew. Chem., Int. Ed.* **2013**, *52*, 13261–13264.
- (20) Roy, R. K.; et al. Design and synthesis of digitally encoded polymers that can be decoded and erased. *Nat. Commun.* **2015**, *6*, 7237.
- (21) Trinh, T. T.; Oswald, L.; Chan-Seng, D.; Lutz, J.-F. Synthesis of molecularly encoded oligomers using a chemoselective 'AB + CD' iterative approach. *Macromol. Rapid Commun.* **2014**, 35, 141–145.
- (22) Porel, M.; Thornlow, D. N.; Phan, N. N.; Alabi, C. A. Sequence-defined bioactive macrocycles via an acid-catalysed cascade reaction. *Nat. Chem.* **2016**, *8*, 590–596.
- (23) Kanasty, R. L.; et al. Sequence-Defined Oligomers from Hydroxyproline Building Blocks for Parallel Synthesis Applications. *Angew. Chem.* **2016**, *128*, *9681*–*9685*.
- (24) Solleder, S. C.; Zengel, D.; Wetzel, K. S.; Meier, M. A. R. A Scalable and High-Yield Strategy for the Synthesis of Sequence-Defined Macromolecules. *Angew. Chem., Int. Ed.* **2016**, *55*, 1204–1207.
- (25) Schneider, R. V.; et al. Sequence-definition in stiff conjugated oligomers. Sci. Rep. 2018, 8, 17483.
- (26) Barnes, J. C.; et al. Iterative exponential growth of stereo- and sequence-controlled polymers. *Nat. Chem.* **2015**, *7*, 810–815.
- (27) Leibfarth, F. A.; Johnson, J. A.; Jamison, T. F. Scalable synthesis of sequence-defined, unimolecular macromolecules by Flow-IEG. *Proc. Natl. Acad. Sci. U. S. A.* **2015**, *112*, 10617–10622.
- (28) Dong, R.; et al. Sequence-defined multifunctional polyethers via liquid-phase synthesis with molecular sieving. *Nat. Chem.* **2019**, *11*, 136
- (29) Siddall, T. H.; Stewart, W. E.; Knight, F. D. Nuclear magnetic resonance studies of hindered internal rotation in higher N,N-dialkylamides and -thionamides. *J. Phys. Chem.* **1970**, *74*, 3580–3583.
- (30) Tong, T.; Ren, N.; Soomi, P.; Wu, J.; Guo, N.; Kang, H.; Kim, E.; Wu, Y.; He, P.; Li, Y.; Tu, B. Electronic Effect on the Molecular Motion of Aromatic Amides: Combined Studies Using VT-NMR and Quantum Calculations. *Molecules* **2018**, *23*, 3382.
- (31) Wang, J.; et al. Counting loops in sidechain-crosslinked polymers from elastic solids to single-chain nanoparticles. *Chemical Science* **2019**, *10*, 5332–5337.
- (32) Zhou, H.; et al. Counting primary loops in polymer gels. *Proc. Natl. Acad. Sci. U. S. A.* **2012**, *109*, 19119–19124.
- (33) Zhou, H.; et al. Crossover experiments applied to network formation reactions: improved strategies for counting elastically inactive molecular defects in PEG gels and hyperbranched polymers. *J. Am. Chem. Soc.* **2014**, *136*, 9464–9470.
- (34) Zhong, M.; Wang, R.; Kawamoto, K.; Olsen, B. D.; Johnson, J. A. Quantifying the impact of molecular defects on polymer network elasticity. *Science* **2016**, 353, 1264–1268.
- (35) Hiemenz, P. C.; Lodge, T. P. Polymer Chemistry; CRC Press, 2007.